J Intell Robot Syst
DOI 10.1007/s10846-017-0486-9

Balancing and Trajectory Tracking of Two-Wheeled Mobile Robot Using Backstepping Sliding Mode Control: Design and Experiments

Nasim Esmaeili · Alireza Alfi · Hossein Khosravi

Received: 27 August 2016 / Accepted: 16 January 2017

Abstract The key attributes of Two Wheeled Balancing Mobile Robots (TWBMRs) are nonholonomic constraints and inherent instability. This paper deals with the problem of balancing and trajectory tracking of TWBMR using backstepping Sliding Mode Controller (SMC). First, the mathematical representation of TWBMR is derived using Lagrangian method by incorporating the dynamics of DC motors. Then, a decoupling approach is applied for simplifying the dynamic equations. The backstepping SMC technique is finally adopted to achieve the balancing and trajectory tracking of the TWBMR, whereas both model uncertainties and exogenous disturbance are taken into account in the controller design methodology. In order to determine the velocity, the trajectory tracking is achieved by the kinematic control, which is a common backstepping controller. For the velocity convergence of TWBMR to the generated desired value, two SMCs are designed, in which the motors voltage are directly controlled as the control laws. Simplicity in practical implementation and control law, ability to overcome uncertainties and appropriate performance are the main advantages of the proposed controller. The effectiveness of the proposed controller is verified through simulation and experimental results.

N. Esmaeili · A. Alfi (✉) · H. Khosravi
Faculty of Electrical and Robotic Engineering, Shahrood University of Technology, Shahrood, 36199-95161, Iran
e-mail: a_alfi@shahroodut.ac.ir

Keywords Balancing mobile robot · Nonholonomic constraint · Trajectory tracking · Two layer sliding mode control

1 Introduction

Nowadays, robotics is one of the advanced fields of technology that provides many services to mankind. Wheeled Mobile Robots (WMRs) as the well-known systems with nonholonomic constraints have been broadly applied in different fields [1]. Two Wheeled Balancing Mobile Robots (TWBMRs) are a typical example of WMR, which is inspired from the inverted pendulum system. Light weight, small footprint, rapid rotation and high maneuverability are the main aspects of the TWBMR. These specifications makes it to really efficient for use in different areas, especially, with too much moving objects, such as parks and factories. Using no fossil fuel and having low noise are of other superiorities of these robots.

TWBMRs are characterized by the ability to balance on two parallel coaxial wheels configured with a chassis, whereas each of which is coupled to a DC motor. This kind of robot is an inherent unstable system with high coupled nonlinear dynamics [2, 3]. Based on this, the primary control purpose of TWBMR is to keep balance and avoid falling, whereas the secondary control goal can be trajectory tracking/tracking the desired speed [4].

Published online: 26 January 2017

Modeling and control of TWBMRs have been extensively studied in the literature [5–7]. In several research works, the linear state feedback controller has been adopted using a linearized model [8, 9]. Consequently, there is a mismatch between the real and nominal models, which easily leads to the system instability by external disturbances. In [10], a nonlinear controller has been also designed to control and stabilize TWBMR. The main shortcoming of the work is that the model uncertainties have not been taken into account in the controller design. Ignoring uncertainties may unbalance or destabilize TWBMR under some circumstances. To handle this problem, some researchers have resorted to robust and adaptive control techniques [11–15]. Although these control methods are able to overcome the uncertainties, but some of them involve complex calculations and high volume of mathematics.

The study of intelligent controllers, such as fuzzy controllers, for TWBMRs has received a considerable attention during the last two decades [16–22]. Design of fuzzy controllers requires expert knowledge to determine the appropriate membership functions. Lack of a systematic control design to provide the membership functions makes design and application of the fuzzy controllers very cumbersome. To address this problem, other intelligent techniques were applied, for example learning algorithms. Due to the inherent instability of TWBMR, a controller must rebalance the robot when disturbances or imbalances occur. However, since the learning time of the online learning algorithms is too long to avoid falling the robots, the online learning cannot be efficient in presence of external disturbances.

Sliding mode control (SMC) is another control strategy that has been successfully used for controlling the robots [23–32]. The key advantages of SMC are insensitivity to parameters variation, independence of external disturbances, quick response and easy implementation. In [23], the SMC was designed for a special form of two-wheeled inverted pendulum. In [24–26], the balancing problem of TWBMR was studied without considering trajectory tracking that causes significant restriction in real world applications. In [27], an adaptive SMC was proposed for self-balancing and yaw rate control of a dynamically two-wheeled human transportation vehicle against system uncertainties. In [28], a coaxial self-balancing robot was developed using two SMC for controlling the motions of the robot. In [29], a discrete-time SMC for trajectory tracking of wheeled mobile robots was presented. In [30], the SMC was used to suppress the swing up behavior, assure the tracking accuracy and enhance the robustness of a mobile robot verified by the simulation results. In [31], an adaptive SMC was designed for a TWMR to achieve trajectory tracking in presence of parameter variations and model uncertainties. The results were verified by the numerical simulations. In [32], a SMC for a class of underactuated mechanical systems was presented without experimental results. Backstepping technique proposed for the kinematic controller is also a common solution for controlling WMRs [33–36]. In this technique, a virtual control law is first defined for a number of the system's outputs. Then, another control method is employed to realize the defined control laws [37].

Having these facts in mind, the main distinctions of the current work in comparison with other related works mentioned above are in the following aspects: (1) the dynamic of DC motors are taken into account in the entire dynamic model to ensure a reliable and meaningful control performance, (2) instead of the torque control strategy, in this paper, the voltage control strategy is applied. Indeed, the generated voltages are directly controlled as the control laws and acts on both wheels, (3) in the proposed control framework, the backstepping SMC is applied for balancing and trajectory tracking of TWBMR. It is worth mentioning that SMC with backstepping technique was only studied in [38], (4) existing literatures on TWBMR mainly consider the SMC technique, but only there exist few experimental results reported, see [27–29]. In addition, the control tasks are achieved only when the TWMRs are placed on a flat surface [23, 27]. In this paper, both simulation and experimental results are given to verify the effectiveness of the proposed controller.

In summary, in this paper, the balancing and trajectory control is achieved simultaneously using the backstepping SMC technique by incorporating a two layer SMC in the core of the proposed control methodology. To this end, the mathematical representation of TWBMR is derived using the Lagrangian method, where the dynamic of DC motors is taken into account in the entire dynamic model. Therefore, the voltages of the motors are directly controlled as the control laws. Experimental results are also provided to illustrate the efficiency of the proposed control scheme.

Fig. 1 Prototype of TWBMR named Zohal

According to our knowledge, this is the first time that the backstepping SMC technique is employed for balancing and trajectory tracking of TWBMR. The main advantages of the proposed controller are the simplicity in practical implementation and control law, appropriate performance and ability to overcome uncertainties. Figure 1 shows the prototype manufacturing of the TWBMR named Zohal. In this figure, the Sony Experia T3 is beyond the robot for better evaluation of the size of WMR, which is 5.3inch.

The rest of this paper is categorized as follows. Mathematical modeling of the robot using Lagrangian method is demonstrated in Section 2. System decomposition is provided in Section 3. Controller design is described in Section 4. Simulation and experimental results are given in Sections 5 and 6, respectively. Finally, Section 7 outlines the main conclusion.

2 Mathematical Modeling

The modeling of a TWBMR is studied in three phases, namely kinematic, dynamic, and actuators modeling. Kinematic modeling describes the geometric relations between the system and mathematics of motion regardless of the affecting mass and forces. Dynamic modeling discusses on the behavior of a system with considering the effect of forces and energies related to chassis. Actuator modeling first derives the relationship between input and output of the actuator and then substitutes these equations into the dynamic equations of the chassis. Schematic diagram of TWBMR is shown in Fig. 2. In Fig. 2, C is position of the center of gravity located in the mid-point of the two wheels, (XYZ) is the reference coordinate frame which is fixed, $(X_rY_rZ_r)$ is the coordinate frame attached to the TWBMR, $(x_c,\ y_c)$ is the coordinates of C in the frame, β is the orientation angle of the TWBMR around the Z-axis, α is the tilt angle of the chassis, θ is the angle of the driving wheels, d is the distance between axle of wheels and the center of gravity, L is the distance between the two driving wheels, and r is the radius of each wheel.

2.1 Kinematic Modeling

The configuration of TWBMR is described by the following six generalized coordinates.

$$q = [x_c\ y_c\ \beta\ \alpha\ \theta_r\ \theta_l]^{\mathrm{T}} \tag{1}$$

where θ_r and θ_l are the angles of the right and left driving wheels, respectively and T denotes the transpose of the corresponding matrix.

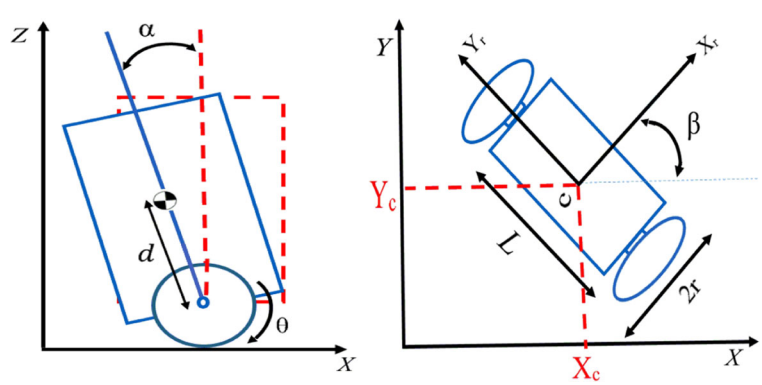

Fig. 2 Schematic diagram of TWBMR with two actuated wheels

The linear velocity in the direction of X_r axis (V_{xr}) and rotational velocity ($\dot{\beta}$) are written as

$$V_{xr} = \frac{r}{2}(\dot{\theta}_r + \dot{\theta}_l) \ , \ \beta = \frac{r}{L}(\dot{\theta}_r - \dot{\theta}_l) \tag{2}$$

where $\dot{\theta}_r$ and $\dot{\theta}_l$ are the angular velocity of the right and left wheels, respectively.

The relationship between Cartesian velocities $\dot{x}_c$ and $\dot{y}_c$ and robot's linear velocity is expressed by

$$\dot{x}_c = V_{xr} \cos\beta \tag{3}$$

$$\dot{y}_c = V_{xr} \sin\beta \tag{4}$$

It is assumed that the movement of TWBMR is pure rolling and no lateral slip, which is stated by the following nonholonomic constraint.

$$\dot{y}_c \cos\dot{\beta} - \dot{x}_c \sin\beta = 0 \tag{5}$$

This equation can be also derived from Eqs. 3 and 4. In addition, two other kinematic constraints can be computed by combination of Eqs. 2–4.

$$\dot{x}_c \cos\beta + \dot{y}_c \sin\beta = r\dot{\theta}_r - \frac{L}{2}\dot{\beta} \tag{6}$$

$$\dot{x}_c \cos\beta + \dot{y}_c \sin\beta = r\dot{\theta}_l + \frac{L}{2}\dot{\beta} \tag{7}$$

The kinematic constraints given in Eqs. 5–7 is represented in the following closed-form.

$$\mathbf{A}(\mathbf{q})\dot{\mathbf{q}} = \mathbf{0} \tag{8}$$

where

$$\mathbf{A}(\mathbf{q}) = \begin{bmatrix} -\sin\beta & \cos\beta & 0 & 0 & 0 & 0 \\ \cos\beta & \sin\beta & \frac{L}{2} & 0 & -r & 0 \\ \cos\beta & \sin\beta & \frac{-L}{2} & 0 & 0 & -r \end{bmatrix}$$

$$\dot{\mathbf{q}} = [\dot{x}_c \quad \dot{y}_c \quad \dot{\beta} \quad \dot{\alpha} \quad \dot{\theta}_r \quad \dot{\theta}_l]^{\mathrm{T}} \tag{9}$$

Kinematic equations also include the Jacobean matrix $\mathbf{J}(\mathbf{q})$. The Jacobean matrix describes the relationship between the time derivative of generalized coordinates ($\dot{q}$) and the velocity of TWBMR.

Let us define the velocity of TWBMR as

$$\mathbf{V} = [\dot{a} \quad V_{xr} \quad \dot{\beta}\,]^{\mathrm{T}} \tag{10}$$

From there,

$$\dot{\mathbf{q}} = \mathbf{J}(\mathbf{q})\,\mathbf{V}$$

$$\mathbf{J}(\mathbf{q}) = \begin{bmatrix} 0 & 0 & 0 & 1 & 0 & 0 \\ \cos\beta & \sin\beta & 0 & 0 & \frac{1}{r} & \frac{1}{r} \\ 0 & 0 & 1 & 0 & \frac{L}{2r} & \frac{-L}{2r} \end{bmatrix}^{\mathrm{T}} \tag{11}$$

In the sequel, the trajectory tracking problem is explained. The goal is to converge the relevant error vector to zero, which can be written in the coordinate frame attached to the robot as

$$\mathbf{e} = \begin{bmatrix} e_x(t) \\ e_y(t) \\ e_\beta(t) \end{bmatrix} = \begin{bmatrix} \cos\beta & \sin\beta & 0 \\ -\sin\beta & \cos\beta & 0 \\ 0 & 0 & 1 \end{bmatrix} \begin{bmatrix} x_d - x \\ y_d - y \\ \beta_d - \beta \end{bmatrix} \tag{12}$$

where $[x_d \ y_d \ \beta_d]^{\mathrm{T}}$ is the desired position of TWBMR.

The time derivative of the error vector is stated as

$$\begin{aligned} \dot{e}_x(t) &= \dot{\beta}\, e_y - V_{xr} + V_{xrd} \cos e_\beta \\ \dot{e}_y(t) &= -\dot{\beta}\, e_x + V_{xr} \sin e_\beta \\ \dot{e}_\beta(t) &= \dot{\beta}_d - \dot{\beta} \end{aligned} \tag{13}$$

where V_{xrd} is the desired linear velocity of the robot along the X_r axis and $\dot{\beta}_d$ is the desired rotational velocity.

2.2 Dynamic Modeling

Here, the energy-based Lagrangian function method is used to derive the dynamic equations of TWBMR. There are two kinds of energies for TWBMR, namely kinetic energy and potential energy. Lagrangian is defined as a difference between the lumped kinematic energy $T$and the lumped potential energy U of the system. This concept is represented as

$$L = T - U \tag{14}$$

and the Lagrangian equation is given by [39]

$$\frac{\mathbf{d}}{\mathbf{dt}}\left(\frac{\partial \mathbf{L}}{\partial \dot{\mathbf{q}}}\right) - \frac{\partial \mathbf{L}}{\partial \mathbf{q}} = \phi + \mathbf{A}(\mathbf{q})^{\mathrm{T}}\boldsymbol{\lambda} \tag{15}$$

where λ is the Lagrangian multiplier and ϕ is the vector of unconstrained generalized forces.

Substituting (14) into (15), the dynamic equations can be described as [40]

$$\mathbf{M}(\mathbf{q})\ddot{\mathbf{q}} + \mathbf{C}(\mathbf{q}, \dot{\mathbf{q}}) = \mathbf{B}(\mathbf{q})\boldsymbol{\tau} + \mathbf{A}(\mathbf{q})^T\boldsymbol{\lambda} \tag{16}$$

where $\mathbf{M}(\mathbf{q})$ is the symmetric positive definite matrix named inertia matrix, $\mathbf{C}(\mathbf{q}, \dot{\mathbf{q}})$ is the centrifugal and Coriolis matrix, $\mathbf{A}(\mathbf{q})$ is the kinematic constraints matrix given in Eq. 10, and $\mathbf{B}(\mathbf{q})$ is the input transformation matrix. Finally, τ denotes the input vector including the right and left motors torque.

$\boldsymbol{\tau}$ and $\mathbf{B}(\mathbf{q})$ given in Eq. 16 are defined as follows.

$$\boldsymbol{\tau} = \begin{bmatrix} \tau_R \\ \tau_L \end{bmatrix} \quad , \quad \mathbf{B}(\mathbf{q}) = \begin{bmatrix} 0 & 0 \\ 0 & 0 \\ 0 & 0 \\ -1 & -1 \\ 1 & 0 \\ 0 & 1 \end{bmatrix} \tag{17}$$

Since it is not easy the calculation of Lagrangian multiplier (λ), it is rational to eliminate this parameter from Eq. 16. It can be performed by pre-multiplication with $\mathbf{J}^{\mathrm{T}}(\mathbf{q})$. Accordingly,

$$\begin{aligned} &\mathbf{J}^{\mathrm{T}}(\mathbf{q})\mathbf{M}(\mathbf{q})\ddot{\mathbf{q}} + \mathbf{J}^{\mathrm{T}}(\mathbf{q})\mathbf{C}(\mathbf{q}, \dot{\mathbf{q}}) \\ &= \mathbf{J}^{\mathrm{T}}(\mathbf{q})\mathbf{B}(\mathbf{q})\boldsymbol{\tau} + \mathbf{J}^{\mathrm{T}}(\mathbf{q})\mathbf{A}(\mathbf{q})^{\mathrm{T}}\boldsymbol{\lambda} \end{aligned} \tag{18}$$

By considering $\mathbf{J}^{\mathrm{T}}(\mathbf{q})\,\mathbf{A}^{\mathrm{T}}(\mathbf{q}) = \mathbf{0}$, we have

$$\mathbf{J}^{\mathbf{T}}\mathrm{T}(\mathbf{q})\mathbf{M}(\mathbf{q})\ddot{\mathbf{q}} + \mathbf{J}^{\mathrm{T}}(\mathbf{q})\mathbf{C}(\mathbf{q}, \dot{\mathbf{q}}) = \mathbf{J}^{\mathrm{T}}(\mathbf{q})\mathbf{B}(\mathbf{q})\boldsymbol{\tau} \tag{19}$$

Taking the time derivative from Eq. 11 leads to

$$\ddot{\mathbf{q}} = \dot{\mathbf{J}}(\mathbf{q})\ \mathbf{V} + \mathbf{J}(\mathbf{q})\,\dot{\mathbf{V}} \tag{20}$$

Substituting (20) into (18) concludes

$$\begin{aligned} &\left(\mathbf{J}^{\mathrm{T}}(\mathbf{q})\mathbf{M}(\mathbf{q})\mathbf{J}(\mathbf{q})\right)\dot{\mathbf{V}} + \mathbf{J}^{\mathrm{T}}(\mathbf{q})\left(\mathbf{M}(\mathbf{q})\dot{\mathbf{J}}\mathbf{V} + \mathbf{C}(\mathbf{q}, \dot{\mathbf{q}})\right) \\ &= \mathbf{J}^{\mathrm{T}}(\mathbf{q})\mathbf{B}(\mathbf{q})\boldsymbol{\tau} \end{aligned} \tag{21}$$

From there,

$$\begin{aligned} \dot{\mathbf{V}} = &-\left(\mathbf{J}^{\mathrm{T}}(\mathbf{q})\mathbf{M}(\mathbf{q})\mathbf{J}(\mathbf{q})\right)^{-1}\mathbf{J}^{\mathrm{T}}(\mathbf{q})\left(\mathbf{M}(\mathbf{q})\dot{\mathbf{J}}\mathbf{V} + \mathbf{C}(\mathbf{q}, \dot{\mathbf{q}})\right) \\ &+\left(\mathbf{J}^{\mathrm{T}}(\mathbf{q})\mathbf{M}(\mathbf{q})\mathbf{J}(\mathbf{q})\right)^{-1}\mathbf{J}^{\mathrm{T}}(\mathbf{q})\mathbf{B}(\mathbf{q})\tau \end{aligned} \tag{22}$$

By defining $\mathbf{X} = [\mathbf{q_p}\ \mathbf{V}]^{\mathrm{T}} = [x_c\ y_c\ \beta\ \alpha\ \dot{\alpha}\ V_{xr}\ \dot{\beta}]^{\mathrm{T}}$ as a state-space vector in which $\mathbf{q_p} = [x_c\ y_c\ \beta\ \alpha]^{\mathrm{T}}$, the dynamic equations can be written in the form of state-space representation as

$$\dot{\mathbf{X}} = \mathbf{f}(\mathbf{x}) + \mathbf{h}(\mathbf{x})\mathbf{u} \tag{23}$$

where

$$\begin{aligned} \mathbf{f}(\mathbf{x}) &= \begin{bmatrix} \mathbf{f_p}(\mathbf{x}) \\ \mathbf{f_v}(\mathbf{x}) \end{bmatrix} \\ &= \begin{bmatrix} \mathbf{J_n}(\mathbf{q})\mathbf{V} \\ -(\mathbf{J}^{\mathrm{T}}(\mathbf{q})\mathbf{M}(\mathbf{q})\mathbf{J}(\mathbf{q}))^{-1}\mathbf{J}^{\mathrm{T}}(\mathbf{q})\mathbf{M}(\mathbf{q})\dot{\mathbf{J}}(\mathbf{q})\mathbf{V} + \mathbf{C}(\mathbf{q}, \dot{\mathbf{q}}) \end{bmatrix} \\ \mathbf{h}(\mathbf{x}) &= \begin{bmatrix} \mathbf{0}_{4\times 2} \\ g_5 \quad g_5 \\ g_6 \quad g_6 \\ g_7 \quad -g_7 \end{bmatrix} = \begin{bmatrix} \mathbf{0}_{4\times 2} \\ (\mathbf{J}^{\mathrm{T}}(\mathbf{q})\mathbf{M}(\mathbf{q})\mathbf{J}(\mathbf{q}))^{-1}\,\mathbf{J}^{\mathrm{T}}(\mathbf{q})\,\mathbf{B}(\mathbf{q}) \end{bmatrix}, \\ \mathbf{u} &= \begin{bmatrix} \tau_R \\ \tau_L \end{bmatrix} \end{aligned} \tag{24}$$

in which

$$\begin{aligned} \mathbf{J_n}(\mathbf{q}) &= \begin{bmatrix} 0 & 0 & 0 & 1 \\ cos\,\beta & sin\,\beta & 0 & 0 \\ 0 & 0 & 1 & 0 \end{bmatrix}^{\mathrm{T}}, \\ \mathbf{J_n}(\mathbf{q})\,\mathbf{V} &= \begin{bmatrix} \dot{x}_c \\ \dot{y}_c \\ \dot{\beta} \\ \dot{\alpha} \end{bmatrix} \end{aligned} \tag{25}$$

2.3 Motor Modeling

The input torques of chassis (τ_R , τ_L) in Eq. 23 are provided via two electric motors. In this subsection, first, the modeling of the DC motor is described. The dynamic of DC motor is then incorporated in the entire dynamic model, where the motor voltages are directly controlled as the control laws. The electrical circuit equations of the DC motor is formulated in the following form.

$$V_m = RI_a + L\dot{I}_a + K_e\dot{\theta}_m \tag{26}$$

$$\tau_m = k_m I_a \tag{27}$$

$$\tau_m = J_m\ddot{\theta}_m + B_m\dot{\theta}_m + r_g\tau_l \tag{28}$$

where R is the rotor resistance, I_a is the armature current, L is the rotor inductance, K_e is the back-emf constant, $\dot{\theta}_m$ is the angular velocity of motor shaft, τ_m and τ_l are the motor torque and load torque, respectively, k_m is torque constant J_m and B_m are the motor inertia and damping coefficient, respectively, and r_g is the gear reduction coefficient.

Due to the small value of parameters L, K_e, J_m and B_m, they can be ignored from the above equations and be comforted in the un-modeled dynamics.

$$V_m = RI_a \tag{29}$$

$$\tau_m = r_g\tau_l \tag{30}$$

From (27), (29) and (30), we have

$$\tau_l = \frac{K_m}{r_g R}V_m \tag{31}$$

Substituting above equation into (23), the motor voltages can be considered as inputs of the system.

$$\mathbf{g}(\mathbf{x}) = \mathbf{h}(\mathbf{x})\frac{K_m}{r_g R} \tag{32}$$

$$\dot{\mathbf{X}} = \mathbf{f}(\mathbf{x}) + \mathbf{g}(\mathbf{x})\mathbf{u} \quad , \quad \mathbf{u} = \begin{bmatrix} V_R \\ V_L \end{bmatrix} \tag{33}$$

where V_R and V_L denote the right and left motor voltages, respectively. $\mathbf{f}(\mathbf{x})$ and $\mathbf{g}(\mathbf{x})$ are also defined in Appendix.

3 System Decomposition

The state-space representation indicates that TWBMR is a high coupled nonlinear system. In the sequel, we decouple the whole system into two separate sub-systems including an inverted pendulum system referred to V_{xr} and α and another system corresponding to the orientation angle of the TWBMR β. The state-space representation of Eq. 23 can be rewritten as

$$\dot{\mathbf{X}} = \begin{bmatrix} f_p(\mathbf{x}) \\ f_5(x) \\ f_6(x) \\ f_7(x) \end{bmatrix} + \begin{bmatrix} 0_{4\times 2} \\ g_5 \;\; 0 \\ g_6 \;\; 0 \\ 0 \;\; g_7 \end{bmatrix} \begin{bmatrix} u_1 \\ u_2 \end{bmatrix} \tag{34}$$

where

$$\begin{aligned} u_1 &= V_R + V_L \\ u_2 &= V_R - V_L \end{aligned} \tag{35}$$

It is straightforward to see that

$$\begin{aligned} V_R &= \frac{1}{2}(u_1 + u_2) \\ V_L &= \frac{1}{2}(u_1 - u_2) \end{aligned} \tag{36}$$

Therefore, the dynamic equations for α, V_{xr}, β can be represented as

$$\begin{aligned} \ddot{\alpha} &= f_5(x) + G_5(x)\, u_1 + d_5(t), \\ \dot{V}_{xr} &= f_6(x) + G_6(x)\, u_1 + d_6(t), \\ \ddot{\beta} &= f_7(x) + G_7(x)\, u_2 + d_7(t). \end{aligned} \tag{37}$$

where $d_5(t)$, $d_6(t)$ and $d_7(t)$ show the bounded lumped disturbances including modeling uncertainty and external disturbances. Here, it is assumed that $|d_5(t)| \le d_{5m}$, $|d_6(t)| \le d_{6m}$ and $|d_7(t)| \le d_{7m}$. In addition, there are nonnegative constants f_{5m}, f_{6m} and f_{7m} such that $|\mathrm{f}_5(t)| \le f_{5m}$, $|\mathrm{f}_6(t)| \le f_{6m}$ and $|\mathrm{f}_7(t)| \le f_{7m}$.

4 Controller Design

In this section, we elaborate the procedure of the controller design. The main purpose of designing the controller is to keep the robot balanced during tracking of the desired trajectory. To achieve these control objectives, two interior control loops are considered as depicted in Fig. 3.

The first one refers to the backstepping technique to guarantee the trajectory tracking of the robot. The second one consists of two SMCs, which are designed to attain the velocity convergence to the generated desired value and keep balancing of the robot. In the current work, a conventional SMC is designed to control the angle of robot in the plane to generate the proper input u_2. A two-layer SMC is also adopted to control the tilt angle and the linear velocity of the robot to construct the appropriate input u_1. In the proposed two-layer SMC, the basic sliding surface is considered as a sum of two other sliding surfaces. Using the proposed control law, the basic sliding surface converges to zero leading to other two sliding surfaces converge to zero.

4.1 Trajectory Tracking

To achieve the trajectory tracking, which is one of the main goals of this paper, the backstepping technique is adopted. For this purpose, the auxiliary velocities control law is introduced as given in Eq. 38 [35].

$$\begin{bmatrix} V_a \\ \dot{\beta}_a \end{bmatrix} = \begin{bmatrix} K_x e_x + V_{xrd} \cos e_\beta \\ \dot{\beta}_d + V_{xrd}\,(K_y e_y + K_\beta \sin e_\beta) \end{bmatrix} ; \quad K_x, K_y > 0 \tag{38}$$

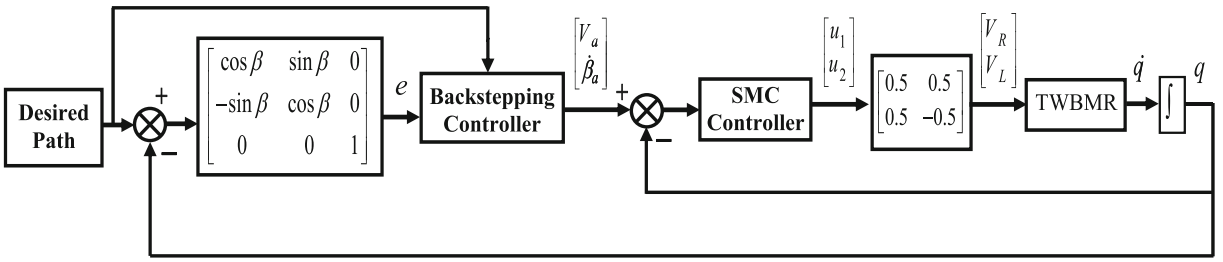

Fig. 3 General control structure

Applying the proposed control law (36), if V and $\dot{\beta}$ converge to V_a and $\dot{\beta}_a$, respectively, then the error vector (12) approaches to zero; that is $e_x \to 0$, $e_y \to 0$, $e_\beta \to 0$, which indicates that the desired trajectory tracking is guaranteed.

4.2 Two Layer SMC

As pointed out in Subsection 4.1, to ensure superior trajectory tracking, the linear velocity V_{xr} and the rotational velocity $\dot{\beta}$ must converge to the auxiliary velocities as given in Eq. 38. Furthermore, in order to keep chassis balance, the tilt angle α must converge to zero. From Eq. 37, it is obvious that $\dot{V}_{xrd}$ and $\ddot{\alpha}$ are under the influence of u_1. Therefore, we can control V_{xr} and α through an appropriate input u_1. Two SMCs are designed including a two-layer SMC corresponding to the coupled system and a traditional SMC for controlling $\dot{\beta}$. First, the sliding surface S is defined as sum of two sliding surfaces namely S_α and S_v to control the chassis tilt angle α and adjust the linear velocity V_{xr} of the robot simultaneously.

$$S = \zeta S_\alpha + \gamma S_v \tag{39}$$

where ζ and γ stand for the sliding mode parameters, which can be constant values or vary according to different conditions, and S_α and S_v are expressed as

$$\begin{aligned} S_\alpha &= \dot{e}_\alpha + \lambda_\alpha e_\alpha \quad ; \quad e_\alpha = \alpha_d - \alpha \\ S_v &= e_v \qquad\qquad ; \quad e_v = V_a - V_{xr} \end{aligned} \tag{40}$$

The purpose of defining S_α is to control the α angle while S_v is defined to regulate the velocity of the robot according to the control law given in Eq. 38.

Theorem 1 [32]. *Using the control law*

$$\begin{aligned} u_1 = &(\zeta g_5 + \gamma g_6)^{-1} \\ &\times [\zeta(\lambda_\alpha \dot{e}_\alpha + \ddot{\alpha}_d - \mathrm{f}_5) + \gamma(\dot{V}_a - \mathrm{f}_6(x)) + \eta \mathrm{sgn}(S_\alpha)] \\ &- k S_\alpha \end{aligned} \tag{41}$$

where η and k are the positive constants and

$$sgn(s) = \begin{cases} 1 & if\ s > 0 \\ 0 & if\ s = 0 \\ -1 & if\ s < 0 \end{cases} \tag{42}$$

$$\gamma = \begin{cases} \gamma_0 & S_\alpha . S_v \geq 0 \\ -\gamma_0 & S_\alpha . S_v < 0 \end{cases} \quad (\gamma_0 > 0) \tag{43}$$

$$\zeta > \frac{\gamma_0 |g_6|}{-g_5} \quad (\gamma_0 > 0) \tag{44}$$

Table 1 Parameters of the TWBMR

Symbol	Value
m_w	0.012kg
r	0.02m
m_b	0.386kg
d	0.065m
l	0.08m

the double-layer sliding surfaces given in Eqs. 39 *and* 40 *is stable, which implies S_α and S_v converge to zero asymptotically.*

4.3 Design of Conventional SMC

Here, we want to design an appropriate control law for the input u_2 to control angular velocity $\dot{\beta}$. The goal of designing this control law is to adjust $\dot{\beta}$ according to Eq. 38. To this end, the following sliding surface is considered.

$$S_2 = e_{\dot{\beta}} \quad ; \quad e_{\dot{\beta}} = \dot{\beta}_a - \dot{\beta} \tag{45}$$

Theorem 2 *Applying the following control law*

$$u_2 = (\frac{1}{g_7})(r_3(t) + \tilde{K}_2 \,\mathrm{sgn}(S_2)) \tag{46}$$

in which

$$\begin{aligned} \tilde{K}_2 = &|\frac{g_7}{\mathrm{Q}_7}|(\gamma_3 + Q_6 + |r_3|) + |r_3|; \\ &|\Delta \mathrm{f}_7| + |d_7(t)| < \mathrm{Q}_6\,, \ |G_7| < \mathrm{Q}_7 \end{aligned} \tag{47}$$

$\dot{\beta}$ converges to the desired value $\dot{\beta}_a$.

Proof Consider the following Lyapunov function.

$$V_3 = \frac{1}{2} S_2^2 \tag{48}$$

Table 2 Parameters of the DC motors

Symbol	Value
R_a	6 [Ω]
L_a	70×10^{-6} [H]
K_m	0.0058 [$\frac{\mathrm{Nm}}{\mathrm{A}}$]
K_e	0.607×10^{-3} [$\frac{\mathrm{V}}{\mathrm{rpm}}$]
J_m	0.66 [g cm^2]
r_g	141:1

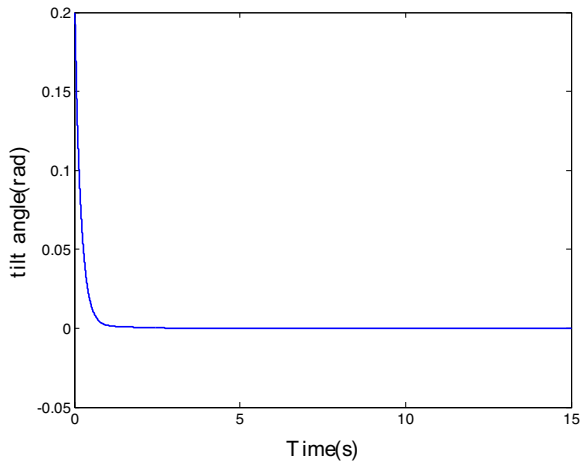

Fig. 4 Tilt angle

Using Eqs. 35 and 36, the time derivative of V_3 is given by

$$\dot{V}_3 = \frac{1}{2} S_2 \dot{S}_2 = S_2(r_3(t) - \Delta f_7 - G_7 u_2) \tag{49}$$

where

$$r_3(t) = \ddot{\beta}_d + \dot{V}_{xrd}\, e_y + V_{xrd}\, \dot{e}_y + \dot{V}_{xrd} \sin e_\beta + V_{xrd}\, \dot{e}_\beta \cos e_\beta - f_7 \tag{50}$$

From Eq. 46, it yields

$$\dot{V}_3 = [r_3(t) - \Delta f_7 - \frac{G_7}{g_7} r_3(t)] S_2 - \frac{G_7}{g_7} K_2 |S_2| \tag{51}$$

From there,

$$\dot{V}_3 \leq (|r_3(t)| + Q_6 + \frac{Q_7}{g_7} |r_3(t)| - \frac{G_7}{g_7} K_2) |S_2| \tag{52}$$

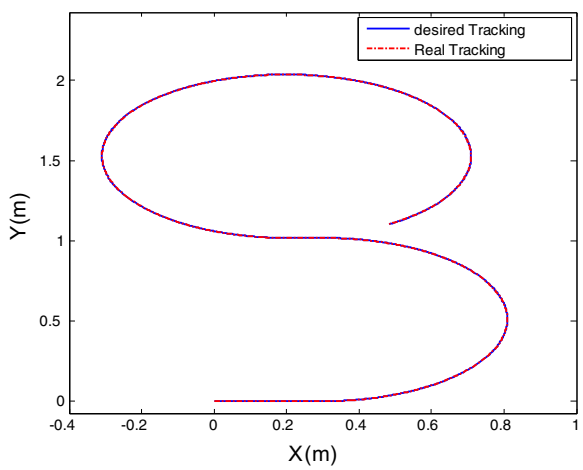

Fig. 5 Tracking pass

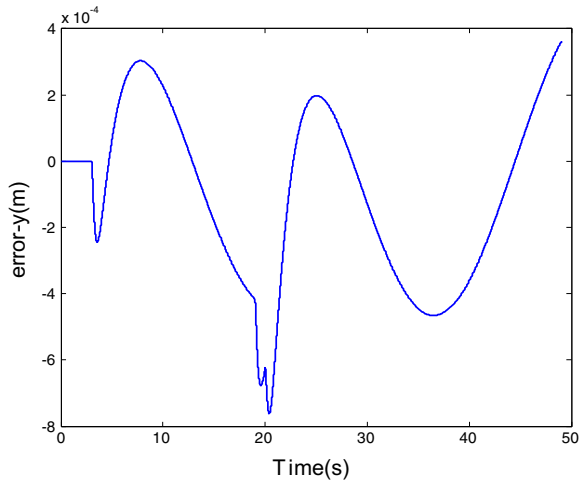

Fig. 6 Tracking error along Y axis

Substituting (47) into (52) with simplification, we have

$$\dot{V}_3 \leq -\gamma_3 |S_2|, \quad \gamma_3 > 0 \tag{53}$$

Therefore, it can be concluded that S_2 goes to zero asymptotically. This completes the proof. □

It is worth mentioning that to attenuate chattering phenomenon, one can replace the sgn(.) by saturation function.

5 Simulation Study

In order to evaluate the performance of the proposed control method, the designed control laws u_1 and u_2

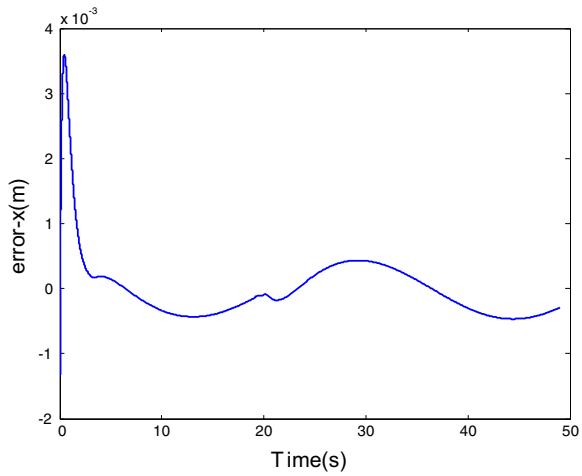

Fig. 7 Tracking error along X axis

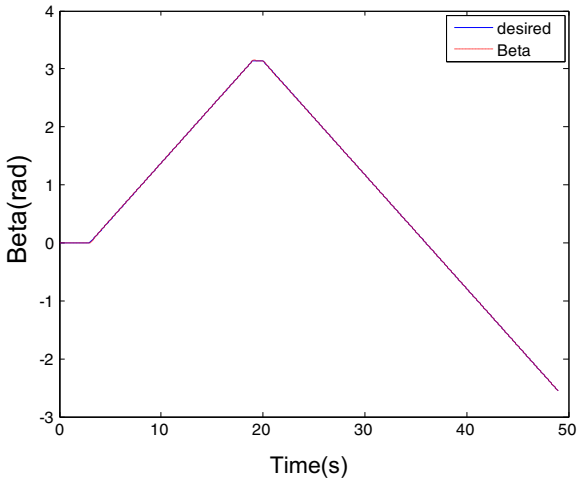

Fig. 8 Tracking profile of β

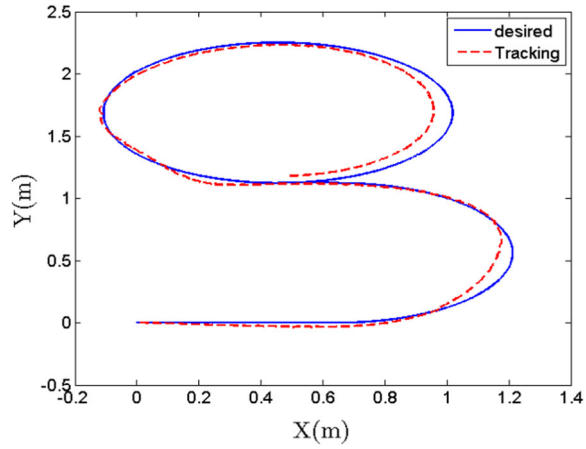

Fig. 10 Real tracking pass

are applied to the dynamic equations of TWBMR in Matlab Simulink. The parameters corresponding to TWBMR and DC motors are listed in Tables 1 and 2, respectively.

In simulation, in order to consider uncertainties and external disturbances, $\mathbf{F}(\mathbf{x})$ and $\mathbf{G}(\mathbf{x})$ are assumed as

$$\mathbf{F}(\mathbf{x}) = \mathbf{f}(\mathbf{x}) + \mathbf{0.1}\sin(\alpha \mathbf{t})\,\mathbf{I}_{3\times 3} \tag{54}$$

$$\mathbf{G}(\mathbf{x}) = \mathbf{g}(\mathbf{x}) + \mathbf{0.3}\sin(\mathbf{t})\,\mathbf{I}_{3\times 3} \tag{55}$$

Results for a curve pass are given in Figs. 4, 5, 6, 7, 8, and 9, where the controller parameters used are $\gamma = 1, k = 1, \zeta = 4, \lambda_a = 0.8, \tilde{K}_2 = 8, \eta = 3$. The tilt angle of robot's chassis approaches to zero asymptotically without any oscillation as shown in Fig. 4. Tilt angle at the time of $0.5sec$ has reached about 0.01 *rad* (equivalent 0.75 *deg*) that is negligible for the balancing robot. In the next times, though robot is on the pass, it well to be able to keep its balance. Figure 4 depicts the desired path and real tracking. Referring to Fig. 5, the performance of the controller in trajectory tracking is satisfactory. The maximum tracking error along x axis is $0.004m$ at the first times. Then, the error reduces and oscillates around $0.0004m$ as shown in Fig. 6. Average error along x axis is 0.0003m. The maximum tracking error along y axis is also $0008m$ as illustrated in Fig. 7. Average error along this axis is $0.0002m$. Figures 8 and 9 display the tracking profile and tracking error corresponding to β. Figure 9 reveals that the rotation angle of the robot is very close to the desired angle of rotation.

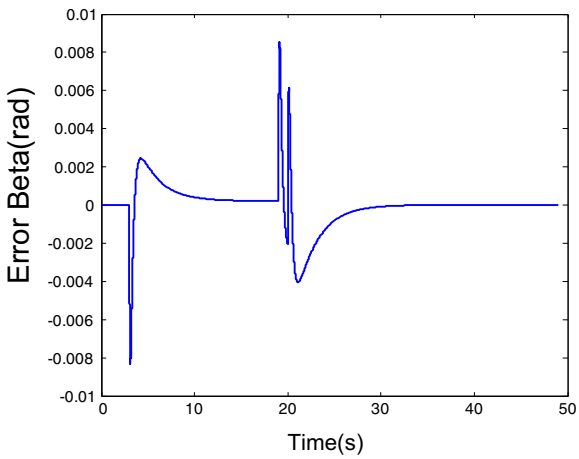

Fig. 9 Tracking error of β

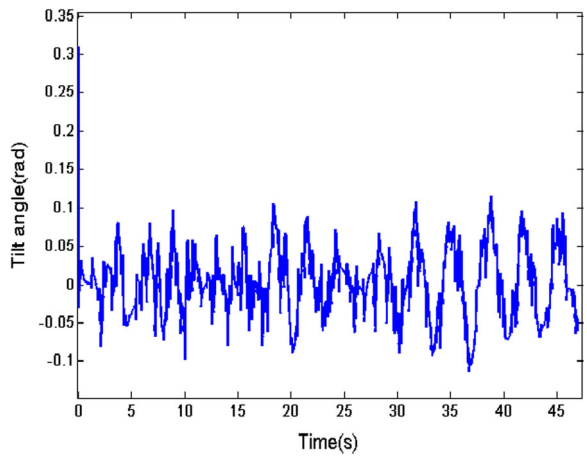

Fig. 11 Real tilt angle

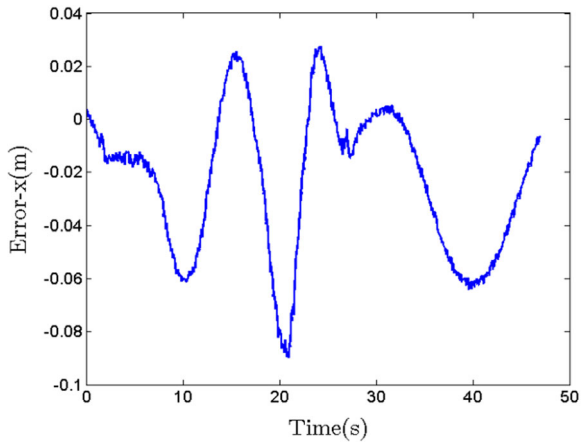

Fig. 12 Real tracking error along X axis

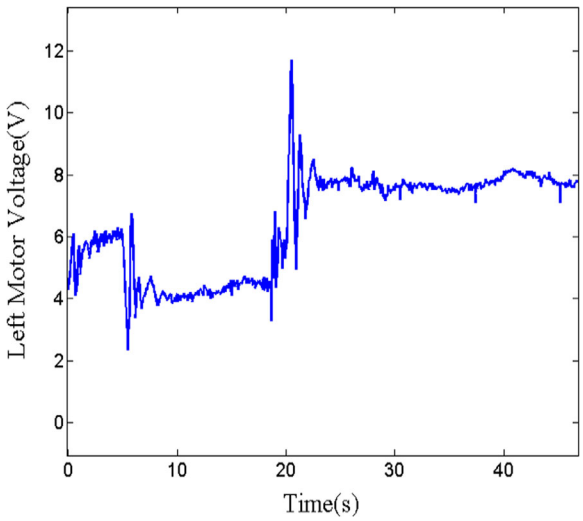

Fig. 14 Left motor voltage

6 Experimental Results

Though results of simulation are satisfactory, the proposed law controls are applied on the Zohal robot for further evaluation of this method. To amend the robot's operation, the designed controller needs to calculate the accurate status of the robot at short sampling time. Situation of robot is defined by tilt angle, angular velocity of tilt angle, Cartesian position of robot in plane, and angular velocity of the robot in plane. To obtain this information, the following instruments are embedded in prototype robot. The TWBMR is structured by a 10GHz frequency TCA 100T to measure tilt angle, a MPU-9150 chip to measure angular velocity of tilt angle, two permanent magnet DC motors with gearboxes and encoders for computing Cartesian position of robot. Also, the robot consists of a processing unit (microcontroller) to receive data from sensors and encoders and then sending them to a computer (PC). The processing unit is an ATMEGA 128AVR. The connection between the microcontroller and PC has been established via a HC-05 V2 Bluetooth interface. After receiving data from robot, the computer computes the output of the controller in MATLAB Simulink and then sends it back to the robot via Bluetooth interface. The HC-05 receives and sends this

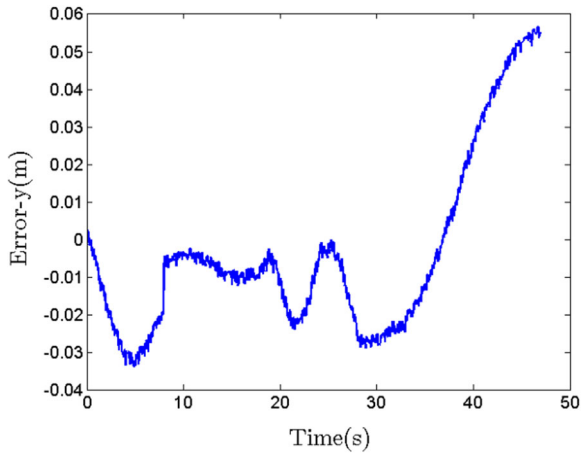

Fig. 13 Real tracking error along Y axis

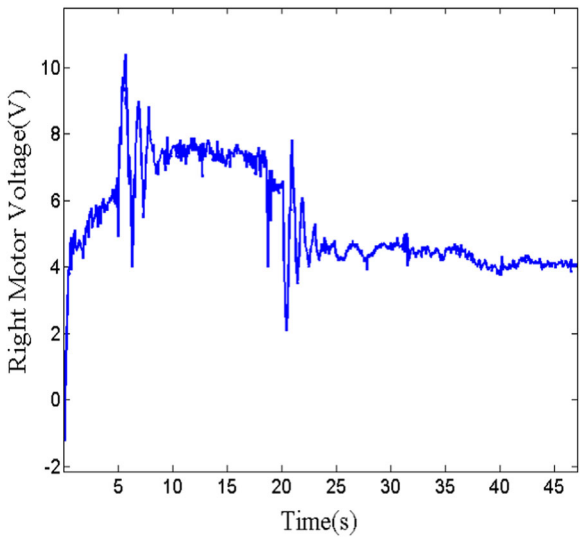

Fig. 15 Right motor voltage

data to the processing unit to produce PWM pulse. Afterward, a L298 chip, which is a motor driver, forwards the generated PWM pulse to the motors. Power supply of robot is a three cell lithium battery, which can apply $11.7v$ to robot's circuits. Corresponding results of practical testing are demonstrated in Figs. 10–15. The tilt angle of robot from an initial value of $0.31rad$ (equivalent $17.7deg$) is reached about $0rad$ in less than one second and stay about 0 during tracking path as shown in Fig. 10. There is slight oscillation in tilt angle about zero that is not sensible in practical implementation. The real tracking path and the tilt angle are represented in Figs. 10 and 11, respectively. The good ability of the proposed controller is visible in these figures. The tracking error along X axis and Y axis are shown in Figs. 12 and 13, respectively. Average of tracking errors along X and Y axes are 0.022 (m) and 0.01 (m), respectively. The output of the controller related to the right and left motors is illustrated in Figs. 14 and 15, respectively. From Figs. 14 and 15, it is apparent that that the outputs voltages are always less than 11.7(V) and never exceed its range.

7 Conclusions

The main purpose of this paper was to address the trajectory tracking and balancing problems of TWBMR using backstepping SMC control strategy. First, the robot dynamic equations were provided by Lagrangian formulation including mathematical model of the permanent magnet DC motors. The SMC in this endeavor was designed to control the voltage of motors instead of robot's torque. Simulation and experimental results were provided to validate the capability of the proposed controller for balancing robot with satisfactory behavior in trajectory tracking problem.

Appendix

In Eq. 33, we have

$$\mathbf{f(x)} = [\mathrm{f}_1(x)\ \mathrm{f}_2(x)\ \mathrm{f}_3(x)\ \mathrm{f}_4(x)\ \mathrm{f}_5(x)\ \ \mathrm{f}_6(x)\ \ \mathrm{f}_7(x)\ ]^{\mathrm{T}}$$

where

$$\mathrm{f}_1(x) = V_{xr}\ \cos\beta$$
$$\mathrm{f}_2(x) = V_{xr}\ \sin\beta$$
$$\mathrm{f}_3(x) = \dot{\beta}$$
$$\mathrm{f}_4(x) = \dot{\alpha}$$
$$\mathrm{f_p}(x) = \begin{bmatrix} \mathrm{f}_1(x) \\ \mathrm{f}_2(x) \\ \mathrm{f}_3(x) \\ \mathrm{f}_4(x) \end{bmatrix}$$

$$\mathrm{f}_5(x) = \frac{dgm_b \sin(\alpha)\left(4m_b r^2 + 2I_{wa} + 2m_w r^2\right) + d^2\dot{\alpha}^2 m_b \sin(2\alpha)\left(3m_b r^2 + 4I_{wa} + 3m_w r^2\right)}{I_b m_b r^2(2I_{wa}+2) + \cos(^2\alpha)d^2 m_b(2I_{wa} + 2m_w r^2) + 2I_b m_w r^2}$$

$$\mathrm{f}_6(x) = \frac{-\left[\left(d^2 m_b^2 r^2\ \left((\sin(2\alpha)\left[3d\dot{\alpha}^2\cos\alpha + \frac{3}{2}g\right]\right) - \dot{\beta}V_{xr}\cos^2\alpha\right)\right) - I_{bg}d\dot{\alpha}^2 r^2 \sin(\alpha)(m_b+2)\right]}{I_b m_b r^2(2I_{wa}+2) + \cos(^2\alpha)d^2 m_b(2I_{wa} + 2m_w r^2) + 2I_b m_w r^2}$$

$$\mathrm{f}_7(x) = \frac{2m_b r^2\left(V_{xr}^2 + d\dot{\alpha}\cos(\alpha)V_{xr}\right)\dot{\beta}}{\left(I_{wa}l^2 + r^2\left(2I_b + m_w l^2 + 2I_b\right)\right.}$$

and

$$\mathbf{g(x)} = \begin{bmatrix} 0 & 0 & 0 & 0 & g_5 & g_6 & g_7 \\ 0 & 0 & 0 & 0 & g_5 & g_6 & g_7 \end{bmatrix}^T$$

where

$$g_5(x) = \frac{-\left(2I_{wa} + dm_b r\cos(\alpha) + r^2(2m_w + 3m_b)\right)}{m_b r^2\left(3I_{by}m_b + 2I^2 m_b m_w\cos^2(\alpha)\right) + 2I_{wa}\left(I_{by} + d^2 m_b\cos^2(\alpha)\right)}$$

$$g_6(x) = \frac{\left(I_{by} + dm_b\ (d\ \cos^2(\alpha) + 3r\cos(\alpha)\right)}{r(3I_{by}m_b + 2d^2 m_b m_w\cos^2(\alpha)) + 2I_{wa}(I_{by} + d_{m_b}^2\cos^2(\alpha))}$$

$$g_7(x) = \frac{r}{l^2(I_{wa} + m_w r^2) + 4I_b r^2 l}$$

References

1. Mohareri, O., Dhaouadi, R., Rad, A.B.: Indirect Adaptive Tracking Control of a Nonholonomic Mobile Robot via Neural Networks. Neurocomput. **88**, 54–66 (2012)
2. Villarreal-Cervantes, M.G., Guerrero-Castellanos, J.F., Ramírez-Martínez, S., Sánchez-Santana, J.P.: Stabilization of a (3,0) Mobile Robot by Means of an Event-Triggered Control. ISA Trans. **58**, 605–613 (2015)
3. Miah, M.S., Gueaieb, W.: Mobile Robot Trajectory Tracking Using Noisy RSS Measurements: An RFID Approach. ISA Trans. **53**, 433–443 (2014)
4. Scaglia, G., Serrano, E., Rosales, A., Albertos, P.: Linear Interpolation Based Controller Design for Trajectory Tracking Under Uncertainties: Application to Mobile Robots. Control Eng. Pract. **45**, 123–132 (2015)
5. Baloh, M., Parent, M.: Modeling and Model Verification of an Intelligence Self-Balancing Two-Wheeled Vehicle for an Autonomous Urban Transportation System. In: Conference on Computational Intelligence, Robotics, and Autonomous Systems, pp. 1–7 (2003)
6. Salerno, A., Angeles, J.: A New Family of Two Wheeled Mobile Robots: Modeling and Controllability. IEEE Trans. Robotics **23**, 169–173 (2007)
7. Kim, Y., Lee, S., Kim, D.H.: Dynamic Equations of a Wheeled Inverted Pendulum with Changing Its Center of Gravity. In: International Conference on Control, Automation and Systems, pp. 8534–854 (2011)
8. Takei, T., Imamura, R., Yuta, S.: Baggage Transportation and Navigation by a Wheeled Inverted Pendulum Mobile Robot. IEEE Trans. Ind. Electron. **56**, 3989–3994 (2009)
9. Junfeng, W., Wanying, Z.H.: Research on Control Method of Two-Wheeled Self-Balancing Robot. In: International Conference on Intelligent Computation Technology and Automation, pp. 476–479 (2011)
10. Pathak, K., Franch, J., Agrawal, S.K.: Velocity and Position Control of a Wheeled Inverted Pendulum by Partial Feedback Linearization. IEEE Trans. Robot. Autom. **21**, 505–513 (2005)
11. Chiu, C.H.: The Design and Implementation of a Wheeled Inverted Pendulum Using an Adaptive Output Recurrent Cerebellar Model Articulation Controller. IEEE Trans. Ind. Electron. **57**, 1814–1822 (2010)
12. Yau, H.T., Wang, C.C., Pai, N.S., Jang, M.J.: Robust Control Method Applied in Self-Balancing Two-Wheeled Robot. In: International Symposium on Knowledge Acquisition and Modeling, pp. 268–271 (2009)
13. Lin, S.C., Tsai, C.C., Huang, H.C.: Nonlinear Adaptive Sliding-Mode Control Design for Two-Wheeled Human Transportation Vehicle. In: IEEE International Conference on Systems, Man, and Cybernetics, pp. 1965–1970 (2009)
14. Wu, J., Liang, Y., Wang, Z.: A Robust Control Method of Two-Wheeled Self-Balancing Robot. In: International Forum on Strategic Technology, pp. 1031–1035 (2011)
15. Wasif, A., Raza, D., Rasheed, W., Farooq, Z., Ali, S.Q.: Design and Implementation of a Two Wheel Self Balancing Robot with a Two Level Adaptive Control. In: IEEE International Conference on Digital Information Management system, Man, and Cybernetics, pp. 187–193 (2013)
16. Pinzon-Morales, R.D., Hirata, Y.: A Portable Stand-Alone Bi-Hemispherical Neuronal Network Model of the Cerebellum for Adaptive Robot Control. In: IEEE International Conference on Robotics and Biomimetics, pp. 1148–1151 (2014)
17. Su, K.H., Chen, Y.Y.: Balance Control for Two-Wheeled Robot via Neural-Fuzzy Technique. In: SICE Annual Conference, pp. 1838–2842 (2010)
18. Wu, J., Jia, S.: T-S Adaptive Neural Network Fuzzy Control Applied in Two-wheeled Self-balancing Robot. In: International Forum on Strategic Technology, pp. 1023–1026 (2011)
19. Chiu, C.H., Lin, Y.W., Lin, C.H.: Real-Time Control of a Wheeled Inverted Pendulum Based on an Intelligent Model Free Controller. Mechatronics **21**, 523–533 (2011)
20. Zeng, W., Wang, Q., Liu, F., Wang, Y.: Learning From Adaptive Neural Network Output Feedback Control of a Unicycle-Type Mobile Robot. ISA Trans. **61**, 337–347 (2016)
21. Dai, Y., Kim, Y., Wee, S.G., Lee, D.H., Lee, S.G.: Symmetric Caging Formation for Convex Polygonal Object Transportation by Multiple Mobile Robots Based on Fuzzy Sliding Mode Control. ISA Trans. **60**, 321–332 (2016)
22. Khooban, M.H., Alfi, A., Maryam Abadi, D.N.: Teaching-Learning-Based Optimal Interval Type-2 Fuzzy PID Controller Design: A Nonholonomic Wheeled Mobile Robots. Robotica **31**, 1059–1071 (2013)
23. Huang, J., Guan, Z.H., Matsuno, T.: Sliding-Mode Velocity Control of Mobile-Wheeled Inverted-Pendulum Systems. IEEE Trans. Robotics **26**, 750–758 (2010)
24. Yau, H.T., Wang, C.C., Paid, N.S., Jang, M.J.: Robust Control Method Applied in Self-Balancing Two-Wheeled Robot. In: International Symposium on Knowledge Acquisition and Modeling, pp. 268–271 (2009)
25. Ghani, N.M.A., Yatim, N.I.M., Azmi, N.A.: Comparative Assessment for Two Wheels Inverted Pendulum Mobile Robot Using Robust Control. In: International Conference on Control, Automation and System, pp. 562–567 (2010)
26. Wu, J., Liang, Y., Wang, Z.: A Robust Control Method of Two-Wheeled SelfBalancing Robot. In: International Forum on Strategic Technology, pp. 1031–1035 (2011)
27. Lin, S.C., Tsai, C.C., Huang, H.C.: Nonlinear Adaptive Sliding-Mode Control Design for Two-Wheeled Human Transportation Vehicle. In: IEEE International Conference on Systems, Man, and Cybernetics, pp. 1965–1970 (2009)
28. Dai, F., Li, F., Bai, Y., Guo, W., Zong, C., Gao, X.: Development of a Coaxial Self-Balancing Robot Based on Sliding Mode Control. In: IEEE International Conference on Mechatronics and Automation, pp. 1241–1246 (2012)
29. Filipescu, A., Minzu, V., Dumitrascu, B., Filipescu, A., Minca, E.: Trajectory-Tracking and Discrete-Time Sliding-Mode Control of Wheeled Mobile Robots. In: IEEE International Conference on Information and Automation, pp. 27–32 (2011)
30. Yue, M., Sun, W., Hu, P.: Sliding Mode Robust Control For Two-Wheeled Mobile Robot With Lower Center of Gravity. International Journal of Innovative Computing, Information and Control **7**, 637–646 (2011)
31. Cui, M., Liu, W., Liu, H., Jiang, H., Wang, Z.: Extended State Observer-Based Adaptive Sliding Mode Control

of Differential-Driving Mobile Robot with Uncertainties. Nonlinear Dyn. **83**, 667–683 (2016)
32. Wang, W., Yi, J., Zhao, D., Liu, X.: Double Layer Sliding Mode Control for Second-order Underactuated Mechanical System. In: IEEE/RSJ International Conference on Intelligent Robots and Systems, pp. 295–300 (2005)
33. Nomura, T., Kitsuka, Y., Suemitsu, H., Matsuo, T.: Adaptive Backstepping Control for a Two-Wheeled Autonomous Robot. In: ICROS SICE International Joint Conference, pp. 4687–4692 (2009)
34. Thao, N., Nghi, D., Phuc, N.: A PID Backstepping Controller For Two-Wheeled Self-Balancing Robot. In: IFOST 2010, pp. 1–6 (2010)
35. Cui, R., Guo, J., Mao, Z.: Adaptive backstepping control of wheeled inverted pendulums models. Nonlinear Dyn. **79**, 501–511 (2015)
36. Kanayama, Y., Kimura, Y., Miyazaki, F., Noguchi, T.: A Stable Tracking Control Method for an Autonomous Mobile Robot. In: IEEE Conference on Robotics Automation, pp. 384–389 (1990)
37. Chan, R., Stol, K., Halkyard, C.R.: Review of Modelling and Control of Two-Wheeled Robots. Annual Reviews in Control **37**, 89–103 (2013)
38. Tsai, C.C., Ju, S.Y., Hsieh, S.M.: Trajectory Tracking of a Self Balancing Two-Wheeled Robot Using Backstepping Sliding-Mode Control and Fuzzy Basis Function Networks. In: IEEE/RSJ International Conference on Intelligent Robots and Systems, pp. 3943–3948 (2010)
39. Ostrovskaya, S., Angeles, J.: Nonholonomic Systems Revisited Within the Framework of Analytical Mechanics. Applied Mechanics Reviews **51**, 415–433 (2009)
40. Pathak, K., Franch, J., Agrawal, S.K.: Velocity and Position Control of a Wheeled Inverted Pendulum by Partial Feedback Linearization. IEEE Trans. Robotics **21**, 505–513 (2005)

Nasim Esmaeili has received his B.Sc. degree in Computer Engineering from Rafsanjan University, Iran, in 2012. He is currently M.Sc. student in Shahrood University of Technology, Shahrood, Iran. Her research focuses on Design and Control of Mechatronic Systems, Wheeled Mobile Robots and Nonlinear Control.

Alireza Alfi has received his B.Sc. degree from Ferdowsi University of Mashhad, Mashhad, Iran, in 2000, and his M.Sc. and Ph.D. degrees from Iran University of Technology, Tehran, Iran, in 2002 and 2007, all in Electrical Engineering. He joined Shahrood University of Technology, Shahrood, Iran in 2008, where he is currently an Associate Professor of Electrical Engineering. His research interests include Control Theory, Teleoperation Systems, Optimization, Heuristic Algorithms and Fractional Calculus.

Hossein Khosravi studied Electronics engineering at Sharif University of Technology in 2003. He received M.Sc. and Ph.D. degrees in Image Processing from Tarbiat Modares University of Iran in 2005 and 2009. Since 2009 he is Assistant Professor at the Faculty of Electrical and Robotics Engineering in Shahrood University of Technology. He was the project manager of several commercial products in the field of OCR and ANPR. His research interests include pattern recognition, OCR, image processing, neural networks, machine vision and classifier combination.